Journal of Materials Chemistry A

Accepted Manuscript

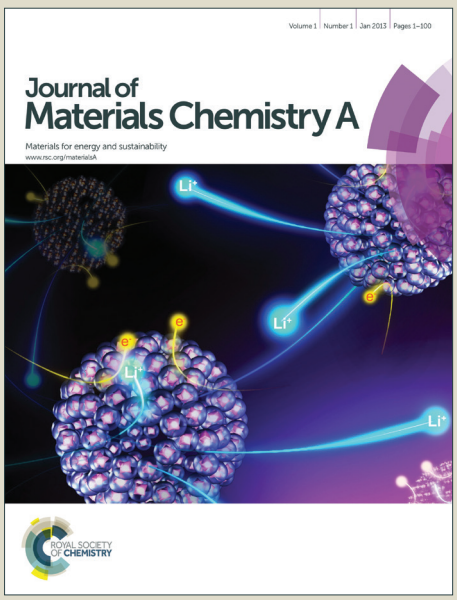

ROYAL SOCIETY OF CHEMISTRY

www.rsc.org/materialsA

TOC Figure

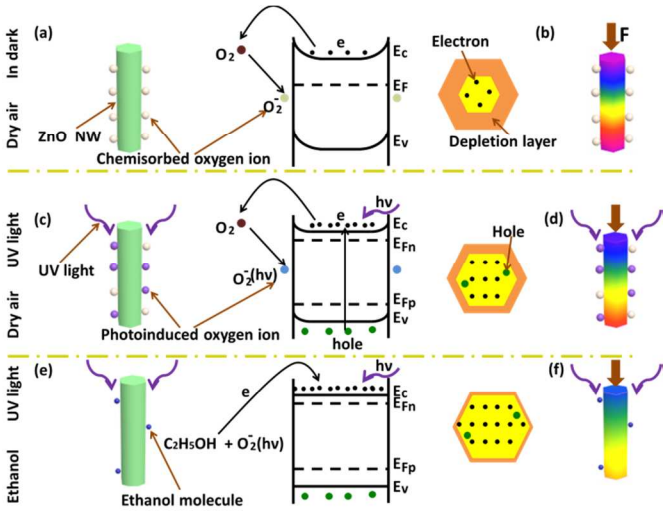

TOC text

Room-temperature self-powered ethanol sensing has been realized from ZnO nanowire arrays by combining their piezoelectric, photoelectric and gas sensing characteristics.

Journal Name

RSCPublishing

ARTICLE

Realizing room-temperature self-powered ethanol sensing of ZnO nanowire arrays by combining their piezoelectric, photoelectric and gas sensing characteristics

Cite this: DOI: 10.1039/x0xx00000x

Received ooth January 2012,
Accepted ooth January 2012

DOI: 10.1039/x0xx00000x

www.rsc.org/

Penglei Wang[a], Yongming Fu[a],Binwei Yu[a], Yayu Zhao[a], Lili Xing[a,], and Xinyu Xue[a,]**

Room-temperature self-powered ethanol sensing has been realized from ZnO nanowire (NW) arrays by combining their piezoelectric, photoelectric and gas sensing characteristics. Under the assistance of UV illumination, the piezoelectric output of ZnO NWs acts not only as a power source, but also as a response signal to ethanol gas at room temperature. Upon exposure to 700 ppm ethanol at room temperature under 67.5 mW/cm^2 UV illumination, the piezoelectric output voltage of ZnO NWs (under 34 N compressive forces) decreases from 0.80 V (in air) to 0.12 V and the response is up to 85. The room-temperature reaction between the UV-induced chemisorbed oxygen ions and ethanol molecules increases the carrier density in ZnO NWs, resulting in a strong piezoelectric screening effect and very low piezoelectric output. Our study can stimulate a research trend on designing new gas sensors and investigating new gas sensing mechanism.

Introduction

Gas sensors have important applications in industrial production, modern agriculture and people's daily life.[1-3] In recent years, the sensitivity and stability of gas sensors have been greatly enhanced by using metal oxide one-dimensional nanostructures due to their high surface-to-volume ratio, such as ZnO nanowires (NWs).[4-7] With the expansion of these nano-sized gas sensors, the development of portable, nano-sized and sustainable power sources for driving these nano-gas sensors is becoming more and more significant.[8-10] In our previous study, an unpackaged ZnO NW nano-generator (NG) as a new self-powered gas sensor has firstly been realized.[11] By coupling the piezoelectric and gas sensing properties of ZnO NWs, the piezoelectric output generated by ZnO NWs acts not only as a power source, but also as a response signal to H_2S gas at room temperature.[12,13] H_2S can react with the adsorbed oxygen ions on ZnO surface and increase the surface carrier density of ZnO, which can strengthen the piezoelectric screening effect and lower the piezoelectric output.[14,15]

On the other hand, restrained by the surface chemical reaction, room-temperature detecting low reducing gas, such as ethanol, can be hardly realized from this new self-powered gas sensor. At room temperature, the chemical reaction between ethanol and oxygen can hardly take place.[16,17] For traditional ethanol sensors, many methods have been used to lower down the work temperature, such as catalyst modification and UV assistance.[18-21] UV illumination on ZnO NWs can increase the free carrier density and influences the adsorption of surface molecules, resulting in room-temperature gas sensing.[22] Thus, if the UV assistance can be introduced into the piezo-gas sensing, then new room-temperature self-powered ethanol sensors can be probably achieved. At the same time, new gas sensing mechanism that combines piezoelectric, photoelectric and gas sensing processes can be established.

In this paper, room-temperature self-powered ethanol sensing has been realized from ZnO nanowire (NW) arrays under the assistance of UV illumination. The room-temperature reaction between the UV-induced oxygen ions and ethanol molecules increases the carrier density in ZnO NWs, resulting in a strong piezoelectric screening effect and lowering down the piezoelectric output. The present results demonstrate a feasible approach for room-temperature self-powered gas sensors.

Experimental

As shown in Fig. 1a, the device is composed of three major components: the ITO glass (indium tin oxide, 2.5×5cm) with ZnO NWs grown on, another piece of ITO glass as the counter electrode (2.5×3.5cm) and transparent PS (Polystyrene) boards as the supporting frame. Two terminal copper leads are glued with silver paste on the two electrodes for electrical measurements, respectively. The uniform ZnO NW arrays on the ITO substrate are synthesized via a simple wet-chemical method. The ITO substrate is cleaned with deionized water and alcohol before the growth of the NWs. The pre-cleaned ITO substrate is deposited with ZnO seeds by a wet-chemical method.[11] The ITO glass is then immersed into 40 mL aqueous solution containing 0.54 g $Zn(NO_3)_2{\cdot}6H_2O$ and 0.35 g hexamethylenetetramine (HMTA). After keeping at 93ºC for 3 hours, the ITO substrate with ZnO NW arrays grown on is removed from the solution, rinsed with deionized water and alcohol, and dried naturally at room temperature.

The schematic diagram of the test system is showed in Fig. 1b. The system is mainly composed of four parts: stepper motor for providing compressive force, gas-flow chamber, UV light and a low-

noise preamplifier. The cylindrical metal bar along the guide rail driven by a stepper motor can apply compressive force on the device. The area of the cylindrical bar (the diameter is about 5 cm) for applying the compressive force is larger than that of the top ITO glass of the device. The cylindrical bar is actuated by the stepper motor moving along the guide rail (the movement of the motor can be precisely controlled by programming, and the repeatability is high). Thus the cylindrical bar can provide stable and uniform deformation on the device for the experimental measurement. The magnitude of the applied force by the cylindrical bar is tested with a standard force sensor. A supporting frame is used for fixing the UV light source and the device in the chamber, which enables the UV light illuminating on the device. The opaque gas-flow chamber is well sealed. The piezoelectric output signal is measured by a low-noise preamplifier (Model SR560, Stanford Research Systems). Under applied compressive force and UV illumination, the piezoelectric output of the device acts as both the power source and the room-temperature ethanol sensing signal.

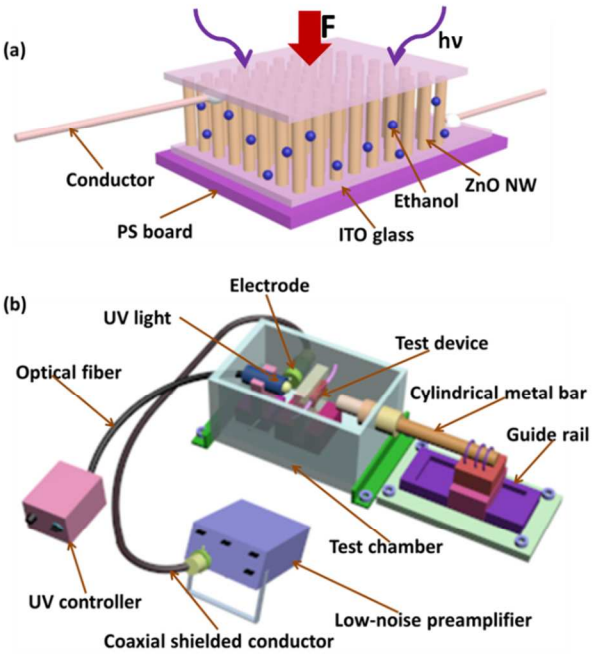

Fig. 1 Fabrication process and measurement setup of the UV-assisted room-temperature self-powered ethanol sensor. (a) The final device structure. (b) The test system.

Characterization

Fig. 2a is a typical SEM image of ZnO NWs from the top view, indicating a good uniformity. The average diameter of ZnO NWs is about 200 nm. A selected area is enlarged in the inset of Fig. 2a, showing that the cross-sectional shape of ZnO NWs is hexagonal. Fig. 2b is a SEM image of ZnO NWs from the side view, revealing that ZnO NWs are vertically aligned on the substrate and the average length of the NWs is about 5.5 um. Fig. 2c is a transmission electron microscopy (TEM) image of a single ZnO NW. It can be seen that the surface of ZnO NWs is very smooth, confirming the high crystalline quality of the as-prepared ZnO NWs. The high-resolution transmission electron microscopy (HRTEM) image and the corresponding select area electron diffraction (SAED) pattern of ZnO NW are shown in Fig. 2d. The as-prepared ZnO nanostructures is single crystalline with a growth direction along the c-axis. The lattice fringe spacing of 0.52 nm corresponds to the (001) plane of the hexagonal wurtzite ZnO nanostructures. A typical X-ray diffraction (XRD) pattern of ZnO NWs is shown in Fig. 2e. The very strong peak marked by pentagram symbol corresponds to the (001) plane of the hexagonal wurtzite ZnO nanostructures. This result can further confirm the uniform growth direction of ZnO NW arrays. Fig. 2f is the EDS spectrum of ZnO NWs on ITO glass, showing that five elements (Zn, O, In, Sn, Si) existed in the selected area. EDS tests also have been carried out at ten other different areas, and the similar results have been obtained, revealing that ZnO NWs are uniformly grown on the ITO glass.

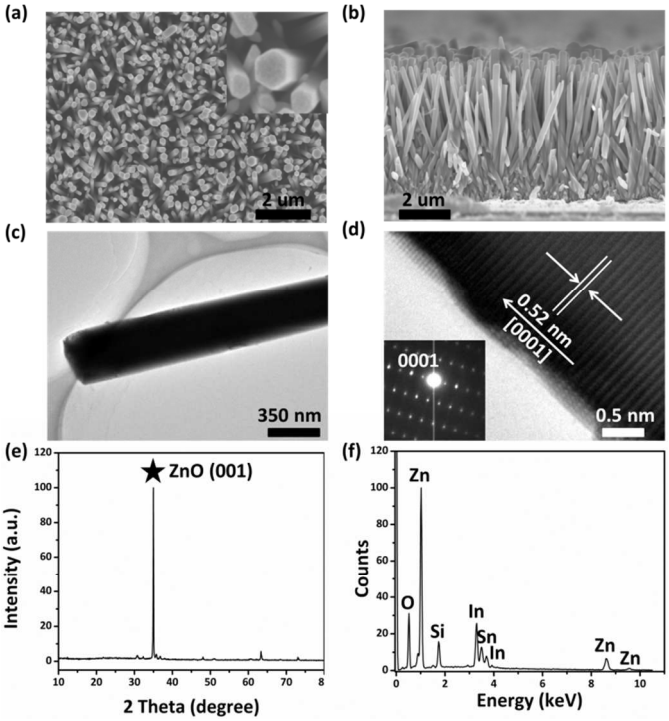

Fig. 2 (a) SEM image of ZnO NW arrays grown on ITO glass from the top view. The inset is an enlarged view. (b) SEM image of ZnO NW arrays grown on ITO glass from the side view. (c) TEM image of one single ZnO NW. (d) HRTEM and SAED pattern of ZnO NW. (e) XRD pattern of ZnO NW arrays grown on ITO glass. (f) EDS spectrum of ZnO NW arrays grown on ITO glass.

Results and discussion

Theoretical working mechanism

Previous studies have shown that the as-prepared ZnO NWs have a high density of point defects, such as oxygen vacancies, which provide n-type carriers (electrons) for the measured conductivity.[23,24] When a compressive force was applied on ZnO NWs, the piezoelectric polarization charges created by the deformation of c-axis can drive electrons in the outside circuit transporting.[25-27] At the same time, the free electrons inside ZnO NWs can also have directional movement to partially screen the piezoelectric polarization charges in the NWs, and the piezoelectric output voltage of NGs is lowered (piezoelectric screening effect).[28,29] The change of carrier density of ZnO and the contact barrier of ZnO/electrode can influence the piezoelectric screening effect and vary the piezoelectric output. For example, the UV illumination on ZnO NG can increase the carrier density of ZnO NW and convert Schottky junction of ZnO/electrode into Ohmic contact, resulting in the decrease of the piezoelectric output.[30] In our previous report, we have demonstrated that oxidizing or reducing gas molecules adsorbed on ZnO surface

can influence the surface carrier density, which can change the screening effect and affect the piezoelectric output.[11] The piezoelectric output of ZnO NWs can act not only as the an power source for driving the system, but also as gas sensing signal for detecting adsorbed gas molecules on the surfaces of ZnO NWs. In this paper, the UV illumination is introduced into this piezo-gas sensing process. Under UV illumination, many photo-generated electrons inside ZnO NWs can react with oxygen molecules and form photo-induced oxygen ions (O_2^-(hν)), which are weakly bounded to ZnO NWs and can be easily removed by ethanol at room temperature, resulting in room-temperature ethanol sensing.[31,32]

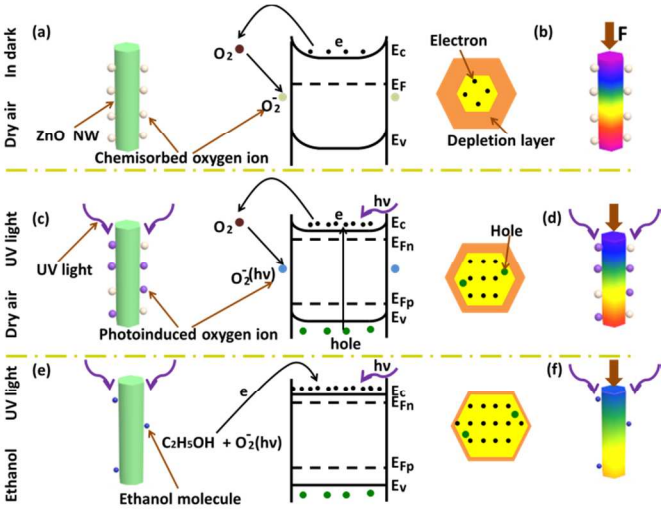

Fig. 3 The working mechanism of the self-powered UV-assisted room-temperature ethanol sensing of ZnO NWs. (a) The device without compressive force in dark and dry air. (b) The piezoelectric output of the device under compressive force in dark and dry air. (c) The device without compressive force under the UV illumination and in dry air. (d) The piezoelectric output of the device under compressive force and UV illumination in dry air. (e) The device without compressive force under the UV illumination and in ethanol. (f) The piezoelectric output of the device under compressive force and UV illumination in ethanol.

The detailed working mechanism of ZnO-based self-powered UV-assisted room-temperature ethanol sensor is shown in Fig. 3. As shown in Fig. 3a, when the device is in dark, dry air and without any compressive force, no piezoelectric field can be created along the ZnO NW. The negative-charged chemisorbed oxygen ions (O_2^-) can be formed through the adsorbed oxygen molecules on the surface of ZnO NW capturing free electrons from the conduction band of ZnO.[33,34] A depletion layer is formed on the surface of ZnO NW, and the surface electron density of ZnO is low. This process leads to the energy band bending upward on the surface of ZnO. As shown in Fig. 3b, when a compressive force is applied on the c-axis of ZnO NW, a piezoelectric field can be created along the ZnO NW.[35] The piezoelectric screening effect is weak due to the low free electron density in ZnO NW, and the piezoelectric output is high. When the device is placed in dark, the chemisorbed oxygen ion is thermally stable at room temperature and difficult to be removed from the surface of ZnO NW due to the large adsorption energy.[31]

As shown in Fig. 3c**,** when the device is under UV illumination in the dry air and without any compressive force, the device has no piezoelectric output. A large number of electron-hole pairs are generated through the electrons in the valence band of ZnO being excited to the conduction band by UV illumination, leaving holes in the valence band. The Fermi level is no longer unified, and the quasi-Fermi level can be simply introduced to present the carrier density (E_{Fn} for electrons and E_{Fp} for holes). The photo-generated holes can migrate to the surface of ZnO NW and react with the chemisorbed oxygen ion, resulting in the desorption of chemisorbed oxygen ions. This process can be simply described as follows:[36]

$$hv \rightarrow h^+ + e^- \quad (1)$$

$$h^+ + O_{2(ad)}^- \rightarrow O_{2(g)} \quad (2)$$

At the same time, photo-generated electrons can combine with oxygen molecules in air, which can form additional photo-induced oxygen ions:[31]

$$O_2 + e^-(hv) \rightarrow O_2^-(hv) \quad (3)$$

This process can also lead to the energy band bending upward at the surface of ZnO. The adsorption and desorption of oxygen molecules on the surface of ZnO NWs can gradually reach a stable equilibrium state. Even though part of the photo-generated electrons combine with the oxygen molecules in air, the carrier density of ZnO under UV illumination is still much higher than that in dark,[31] and the width of the surface depletion layer decreases. When a compressive force is applied on the device under UV illumination in dry air, a piezoelectric field is created along the ZnO NWs (Fig. 3d). The piezoelectric screening effect is strong due to the high carrier density, and the piezoelectric output voltage of the device is low.

As shown in Fig. 3e, when the device under UV illumination without any compressive force is exposed to ethanol gas, the device has no piezoelectric output. The photo-induced oxygen ions are weakly bounded to ZnO NW and can be easily removed.[31] At room temperature, the ethanol molecules can react with the photo-induced oxygen ions on the surface of ZnO NW as follows:[37,38]

$$CH_3CH_2OH(gas) \leftrightarrow CH_3CH_2OH(ads.) \quad (4)$$

$$CH_3CH_2OH(ads.) \leftrightarrow CH_3CH_2O(ads.) + H(ads.) \quad (5)$$

$$4H(ads.) + O_2^-(hv) \leftrightarrow 2H_2O(gas) + e^- \quad (6)$$

In this process, a large number of free electrons can be released back to the conduction band of ZnO, thus the band bends downward on the surface. The carrier density of ZnO increases and the surface depletion layer width decreases. When a compressive force is applied on the device (Fig. 3f), a piezoelectric field is created along the ZnO NW. The large amount of the free carriers in ZnO NWs can lead to a very strong piezoelectric screening effect, and the piezoelectric output is very low.

On the other hand, the change of barrier height of ZnO/ITO interface can probably contribute to the self-powered UV-assisted room-temperature ethanol sensing of ZnO NWs. As shown in the I-V measurement below, the presence of a Schottky barrier between the ITO electrode and the ZnO NWs plays a very important role for determining the electrical performance of the device. The barrier height of ZnO/ITO interface is determined by the surface states of ZnO NWs because of the Fermi level pinning at surface states.[39] When the device is in dark and dry air, chemisorbed oxygen ions are formed on the surface of ZnO, leading to a large amount of surface states. The Schottky barrier is formed in the ZnO/ITO contact region. When the device is illuminated by UV in dry air, photo-generated electron-hole pairs are generated and separated near the Schottky interface.[39] The desorption of oxygen molecules on the surface of

ZnO NWs can decreases the surface states, and the Schottky barrier height decreases. Thus the piezoelectric output is lowered, which is similar to the previous report.[30] Under UV illumination, when the device is exposed to ethanol gas, the ethanol molecules can react with the photo-induced oxygen ions. The Schottky barrier height is further decreased and the piezoelectric output is very low.

Experimental data and analysis

As shown in Fig. 4, room-temperature UV-assisted self-powered ethanol sensing of ZnO NW arrays has been realized, and the UV illumination plays a critical role in the sensing process. In dark (from 0 to 175 s), the piezoelectric output of the device under compressive force (34 N, 0.4 Hz) has no response to dry air and ethanol at room temperature. As the ethanol concentration increases from 0 to 300, 400 and 500 ppm, the piezoelectric output of the device keeps at about 0.44 V and almost have no changes. Under UV illumination (310 nm, 67.5 mW/cm^2, from 175 to 368 s), the piezoelectric output voltage of the device under compressive force decreases with increasing ethanol concentration. As the ethanol concentration is 100, 200, 300 and 400 ppm, the piezoelectric output voltage of the device is 0.36, 0.23, 0.15 and 0.14 V. These results confirm that room-temperature self-powered ethanol sensing of ZnO can be achieved with the assistance of UV illumination. And this experimental data can well support the above theoretical mechanism.

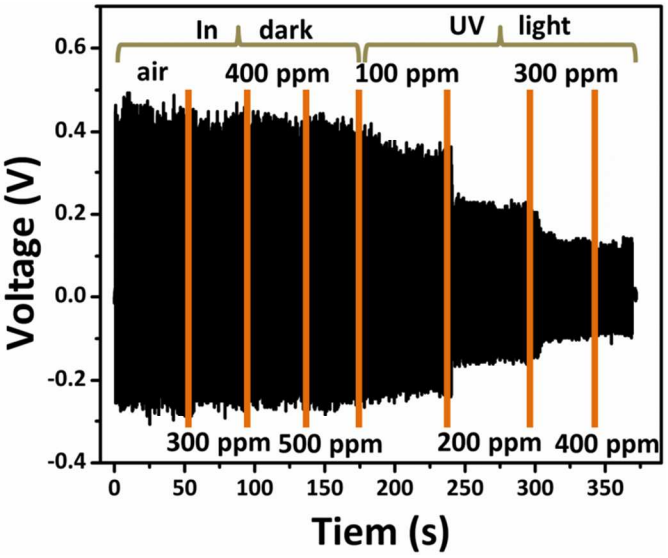

Fig. 4 The UV light plays a critical role in the room-temperature self-powered ethanol sensing. In dark, the piezoelectric output of the device under compressive force has no response to dry air and ethanol at room temperature. Under UV illumination, the piezoelectric output voltage of the device under compressive force decreases with increasing ethanol concentration.

Fig. 5 shows the I–V characteristics of the device in different conditions without compressive force at room temperature, which confirms that the carrier density of ZnO and the contact barrier of ZnO/ITO can be influenced by UV illumination and ethanol. In dark, the conductance of the device is very low, and the I-V curves of the device in dry air, 300, 400 and 500 ppm ethanol at room temperature almost overlap. In dark, the reaction between ethanol and chemisorbed oxygen ions cannot take place at room temperature, and the carrier density cannot be influenced by ethanol concentration in this case. Under UV illumination, the conductance of the device increases with increasing ethanol concentration. Under UV illumination, the reaction between ethanol and photo-induced oxygen ions can take place at room temperature, and the carrier density increases with increasing ethanol concentration. The Schottky barrier decreases at the same time. These results further confirm that the UV illumination and ethanol play important roles in the change of carrier density in ZnO NWs and the contact barrier of ZnO/ITO, supporting the above theoretical mechanism.

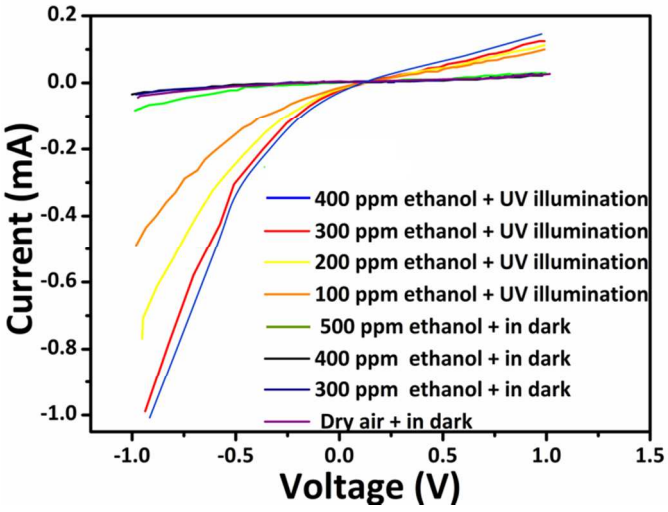

Fig. 5 Typical *I–V* characteristics of the device in different conditions without compressive force at room temperature.

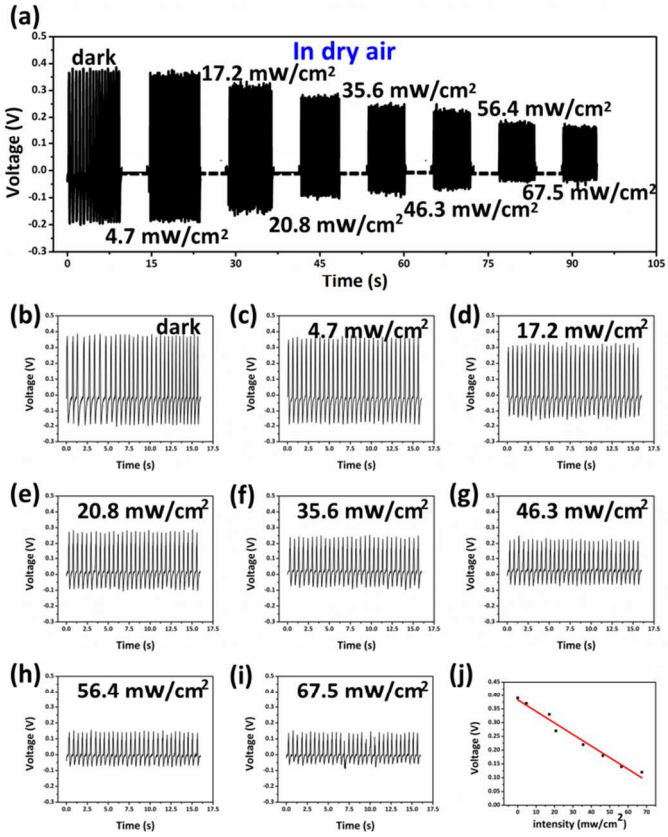

Fig. 6 (a) The piezoelectric output of the device in dry air under different UV intensity. The enlarged piezoelectric output voltage of the device in (b) Dark, (c) 4.7 mW/cm^2, (d) 17.2 mW/cm^2, (e) 20.8 mW/cm^2, (f) 35.6 mW/cm^2, (g) 46.3 mW/cm^2, (h) 56.4 mW/cm^2 and (i) 67.5 mW/cm^2. (j) The relationship between the piezoelectric output and the intensity of the UV light.

The piezoelectric output of the device under compressive force (34 N, 0.4 Hz) in dry air under different UV intensity is shown in Fig. 6a. As shown in Fig. 6b-i, the piezoelectric output voltage of the device in dark, under 4.7, 17.2, 20.8, 35.6, 46.3, 56.4, and 67.5 mW/cm^2 UV illuminations is about 0.39, 0.37, 0.33, 0.27, 0.22, 0.18, 0.14, and 0.12 V, respectively. The piezoelectric output decreases with increasing UV intensity, as shown in Fig. 6j. As the UV intensity increases, a large amount of free carriers are photo-generated and the contact barrier decreases, resulting in strengthening the piezoelectric screening effect and lowering the piezoelectric output. This result can support the above theoretical mechanism.

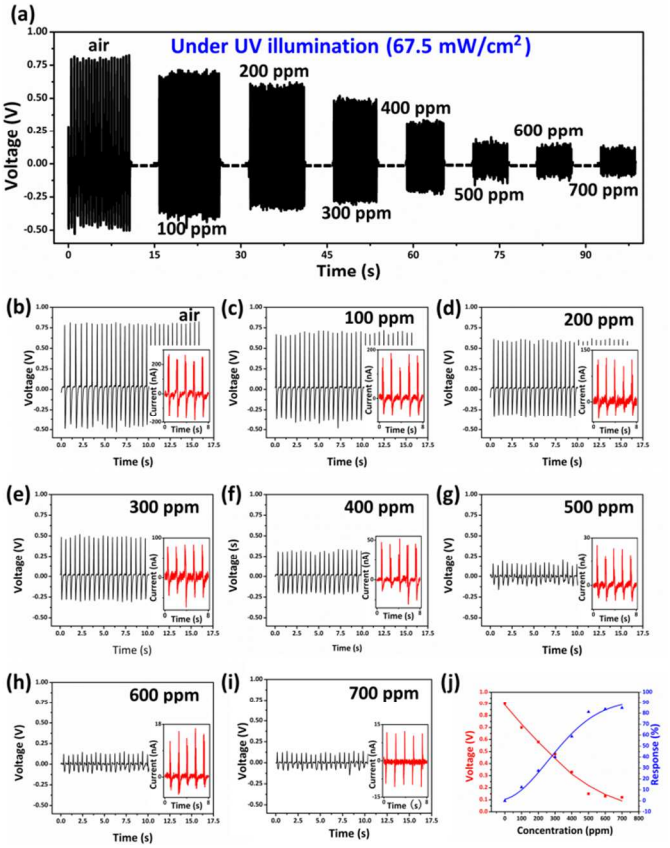

Fig. 7 (a) The piezoelectric output of the device in different ethanol concentration under UV illumination. The output voltage and current of the device in (b) dry air (c) 100 ppm, (d) 200 ppm, (e) 300 ppm, (f) 400 ppm, (g) 500 ppm, (h) 600 ppm and (i) 700ppm ethanol. (j) The voltage-concentration profile and the response.

The room-temperature ethanol sensing performance of ZnO-based UV-assisted self-powered gas sensor is carefully investigated, as shown in Fig. 7. The piezoelectric output of the device under UV illumination (310 nm, 67.5 mW/cm^2) and compressive force (34 N, 0.4 Hz) upon exposure to different ethanol concentration is shown in Fig. 7a. As shown in Fig. 7b-i, the piezoelectric voltages of the device under UV illumination at room temperature upon exposure to dry air, 100, 200, 300, 400, 500, 600 and 700 ppm ethanol is about 0.8, 0.7, 0.58, 0.48, 0.33, 0.15, 0.13 and 0.12 V, respectively. The piezoelectric output current of the device under UV illumination at room temperature upon exposure to dry air, 100, 200, 300, 400, 500, 600 and 700 ppm ethanol is about 248, 168, 120, 80, 47, 23, 15 and 11 nA, respectively. And the power of the device can be evaluated to be 198.40, 117.60, 69.60, 38.40, 15.51, 3.45, 1.95 and 1.32 nW, respectively. It should be pointed that the outputted power of our device with hard ITO glass as the substrates is relatively low. Many previous literatures have reported that the outputted power of NGs can be enhanced by using flexible substrates due to the deformation issue.[40-42] Thus in the future work, research effort can be made on replacing the hard substrates of the device with flexible transparent conducting substrates. As shown in Fig. 7j, the piezoelectric output voltage decreases with increasing ethanol concentration. As the ethanol concentration increases, the free carrier density in ZnO NWs increases arising from the reaction between the photo-induced oxygen ions and ethanol molecules. The contact barrier of ZnO/ITO decreases. These lead to strong piezoelectric screening effect and low piezoelectric output. The piezoelectric output of the device under UV illumination is depended on the concentration of ethanol, demonstrating a feasible approach for realizing room-temperature ethanol sensing.

Similar to the traditional definition of the sensitivity of gas sensors ($S\%=\frac{|R_a-R_g|}{R_a}\times 100\%$, where R_a and R_g represent the resistance of the sensor in dry air and in the test gas, respectively),[43] the response of the self-powered room-temperature ethanol sensor under UV illumination can be simply presented as follows:

$$Response\% = \frac{|V_0-V_i|}{V_0}\times 100\%$$

, where V_0 and V_i are the piezoelectric output of the device in dark and ethanol. Upon exposure to 100, 200, 300, 400, 500, 600 and 700 ppm ethanol, the response of the device is 12.50, 27.50, 40.00, 58.75, 81.25, 83.75 and 85.00, respectively (Fig. 7j). A quasi-linear relationship between the response and the ethanol concentration can be observed with the ethanol concentration lower than 500 ppm, which is a very efficient feature for practical applications. With increasing ethanol concentration, more ethanol molecules can react with the photo-induced oxygen ions, causing more oxygen molecules to be desorbed from the surface of ZnO NWs. As the ethanol concentration is larger than 500 ppm, the saturation of response can be observed, which is similar to that for traditional gas sensors, arising from the competition between the adsorption sites versus the ethanol concentration.[11]

The comparision of various room-temperature self-powered gas sensors is shown in Table 1. Room-temperature gas sensing has been achieved in this series of work through the coupling of the piezoelectric effect and gas sensing characteristics of ZnO NWs. And these gas sensors can operate independently without the use of external electricity storage/supply systems. It can be seen that higher response (after normalizing the definition of response) has been obtained in this work by the UV assistance than the previous results.

Table 1 Comparison of various room-temperature self-powered gas sensors.

Materials	Sensing type	Gas	Concentration	Response	Reference
SnO_2/ZnO	Piezoelectric	H_2	800 ppm	83%	44
CeO_2/ZnO	Piezoelectric	H_2O	95% RH	82%	45
CdS	Piezoelectric	H_2S	600 ppm	63%	46
ZnO	Piezoelectric	H_2S	1000 ppm	56%	11
CuO/ZnO	Piezoelectric	H_2S	800 ppm	86%	47
In_2O_3/ZnO	Piezoelectric	H_2S	700 ppm	90%	48
Pd/ZnO	Piezoelectric	C_2H_5OH	800 ppm	52%	18
Au/ZnO	Piezoelectric	C_2H_5OH	1200 ppm	72%	19
Pt/ZnO	Piezoelectric	C_2H_5OH	1500 ppm	38%	20
ZnO	UV+Piezoelectric	C_2H_5OH	700 ppm	85%	This

Conclusion

In summary, room-temperature ethanol sensing was obtained from ZnO-based UV-assisted self-powered gas sensor. Under externally applied compressive force and UV illumination, the piezoelectric output generated by ZnO NWs acted not only as a power source, but also as a response signal to ethanol at room temperature. Such performance was attributed to the combination of piezoelectric, photoelectric and gas sensing characteristics of ZnO NWs. Our study could stimulate a research trend on designing new gas sensors and investigating new gas sensing mechanism

Acknowledgements

This work was supported by the National Natural Science Foundation of China (51102041 and 11104025), the Fundamental Research Funds for the Central Universities (N120205001 and N120405010), and Program for New Century Excellent Talents in University (NCET-13-0112).

Notes and references

[a] College of Sciences, Northeastern University, Shenyang 110004, China
E-mail addresses: xuexinyu@mail.neu.edu.cn; xingrenyier@sina.com

1 Y. X. Liu, J. Parisi, X. C. Sun and Y. Lei, *J. Mater. Chem. A*, 2014, **2**, 9919-9943.
2 J. S. Lee, O. S. Kwon, D. H. Shin and J. Jang, *J. Mater. Chem. A*, 2013, **1**, 9099-9106.
3 J. Gao, L. Wang, K. Kan, S. Xu, L. Jing, S. Liu, P. Shen, L. Li and K. Shi, *J. Mater. Chem.A*, 2014, **2**, 949-956.
4 L. Shi, C. H. Yu and J. H. Zhou, *J. Phys. Chem. B*, 2005, **109**, 22102-22111.
5 Y. S. Li, J. Xu, J. F. Chao, D. Chen, S. X. Ouyang, J. H. Ye and G. Z. Shen, *J. Mater. Chem.*, 2011, **21**, 12852-12857.
6 X. J. Luo, Z. Lou, L. L. Wang, X. J. Zheng and T. Zhang, *New. J. Chem.*, 2014, **38**, 84-89.
7 S. Bai, S. Chen, Y. Zhao, T. Guo, R. Luo, D. Li and A. Chen, *J.Mater. Chem. A*, 2014, **2**, 16697-16706.
8 S. Mao, G. H. Lu and J. H. Chen, *J. Mater. Chem. A*, 2014, **2**, 5573-5579.
9 J. Kong, N. R. Franklin, C. W. Zhou, M. G. Chapline, S. Peng, K. J. Cho and H. J. Dai, *Science*, 2000, **287**, 622-625.
10 J. Li, Y. J. Lu, Q. Ye, M. Cinke, J. Han and M. Meyyappan, *Nano Lett.*, 2003, **3**, 929-933.
11 X. Y. Xue, Y. X. Nie, B. He, L. L. Xing, Y. Zhang and Z. L. Wang, *Nanotechnology*, 2013, **24**, 225501.
12 J. H. Song, J. Zhou and Z. L. Wang, *Nano Lett.*, 2006, **6**, 1656-1662.
13 Y. T. Chang, J. Y. Chen, T. P. Yang, C. W. Huang, C. H. Chiu, P. H. Yeh and W. W. Wu, *Nano Energy*, 2014, **8**, 291-296.
14 H. S. Woo, C. H. Kwak, I. D. Kim and J. H. Lee, *J.Mater. Chem. A*, 2014, **2**, 6412-6418.
15 N. Jalali, P. Woolliams, M. Stewart, P. M. Weaver, M. G. Cain, S. Dunn and J. Briscoe, *J. Mater. Chem. A*, 2014, **2**, 10945-10951.
16 C. L. Zhu, H. L. Yu, Y. Zhang, T. S. Wang, Q. Y. Ouyang, L. H. Qi, Y. J. Chen and X. Y. Xue, *Acs Appl. Mater. Interfaces*, 2012, **4**, 665-671.
17 P. G. Hu, G. J. Du, W. J. Zhou, J. J. Cui, J. J. Lin, H. Liu, D. Liu, J. Y. Wang and S. W. Chen, *Acs Appl. Mater. Interfaces*, 2010, **2**, 3263-3269.
18 Y. J. Lin, P. Deng, Y. X. Nie, Y. F. Hu, L. L.Xing, Y. Zhang and X. Y. Xue, *Nanoscale*, 2014, **6**, 4604-4610.
19 L. L. Xing, Y. F. Hu, P. L. Wang, Y. Y. Zhao, Y. X. Nie, P. Deng and X. Y. Xue, *Appl. Phys. Lett.*, 2014, **104**.
20 Y. Y. Zhao, X. Lai, P. Deng, Y. X. Nie, Y. Zhang, L. L. Xing and X. Y. Xue *Nanotechnology,* 2014, **25**, 115502.
21 H. Kudo, M. Sawai, X. Wang, T. Gessei, T. Koshida, K. Miyajima, H. Saito and K. Mitsubayashi, *Sensor. Actuat. B-Chem.*, 2009, **141**, 20-25.
22 M. R. Alenezi, A. S. Alshammari, K. D. G. I. Jayawardena, M. J. Beliatis, S. J. Henley and S. R. P. Silva, *J. Phys. Chem. C*, 2013, **117**, 17850-17858.
23 S. Bai, T. Guo, Y. Zhao, R. Luo, D. Li, A. Chen and C. C. Liu, *J. Mater. Chem. A*, 2013, **1**, 11335-11342.
24 A. Janotti and C. G. Van de Walle, *Appl. Phys. Lett.*, 2005, **87**, 122102
25 Z. L. Wang, *Acs Nano*, 2008, **2**, 1987-1992.
26 X. D. Wang, J. Zhou, J. H. Song, J. Liu, N. S. Xu and Z. L. Wang, *Nano Lett.*, 2006, **6**, 2768-2772.
27 Z. L. Wang, *Mater. Today*, 2007, **10**, 20-28.
28 M. Y. Choi, D. Choi, M. J. Jin, I. Kim, S. H. Kim, J. Y. Choi, S. Y. Lee, J. M. Kim and S. W. Kim, *Adv. Mater.*, 2009, **21**, 2185.
29 X. D. Wang, *Nano Energy*, 2012, **1**, 13-24.
30 J. Liu, P. Fei, J. Song, X. Wang, C. Lao, R. Tummala and Z. L. Wang, *Nano Lett.*, 2008, **8**, 328-332.
31 T. I. Barry and F. S. Stone, *Proc. R. Soc. Lond. A*, 1960, **255**, 124.
32 S. W. Fan, A. K. Srivastava and V. P. Dravid, *Appl. Phys. Lett.*, 2009, **95**, 142106.
33 F. Chaabouni, M. Abaab and B. Rezig, *Sensor. Actuat. B-Chem.*, 2004, **100**, 200-204.
34 Z. Y. Fan, D. W. Wang, P. C. Chang, W. Y. Tseng and J. G. Lu, *Appl. Phys. Lett.*, 2004, **85**, 5923-5925.
35 Z. L. Wang and J. H. Song, *Science*, 2006, 312, 242-246.
36 D. A. Melnick, *J. Chem. Phys.*, 1957, **26**, 1136.
37 R. Bajpaia, A. Motayed, A. V. Davydovb, V. P. Oleshkob, G. S. Alurib, K. A. Bertnesse, M. V. Raod and M. E. Zaghloula, *Sensor. Actuat. B-Chem.,* 2012, **171**, 499-507.
38 M. Bowker and R.J. Madix, *Surf. Sci.,* 1982,**116**, 549-572.
39 G. Cheng, X. Wu, B. Liu, B. Li, X. Zhang and Z. Du, *Appl. Phys. Lett.*, 2011, **99**.
40 A. Khan, M. A. Abbasi, M. Hussain, Z. H. Ibupoto, J. Wissting, O. Nur and M. Willander, *Appl. Phys. Lett.*, 2012, **101**.
41 H. Sun, H. Tian, Y. Yang, D. Xie, Y. C. Zhang, X. Liu, S. Ma, H. M. Zhao and T. L. Ren, *Nanoscale*, 2013, **5**, 6117-6123.
42 Y. K. Fuh, J. C. Ye, P. C. Chen and Z. M. Huang, *J. Mater. Chem. A*, 2014, **2**, 16101-16106.
43 M. S. Wagh, G. H. Jain, D. R. Patil, S. A. Patil and L. A. Patil, *Sensor. Actuat. B-Chem.*, 2006, **115**, 128-133.
44 Y. M. Fu, W. L. Zang, P. L. Wang, L. L. Xing, X. Y. Xue and Y. Zhang, *Nano Energy,* 2014, **8**, 34-43.
45 D. Zhu, Y. M. Fu, W. L. Zang, Y. Y. Zhao, L. L. Xing and X. Y. Xue, *Sensor. Actuat. B-Chem.*, 2014, **205**, 12-19.
46 P. L. Wang, P. Deng, Y. X. Nie, Y. Y. Zhao, Y. Zhang, L. L. Xing and X. Y. Xue, *Nanotechnology*, 2014, **25**, 075501.
47 Y. X. Nie, P. Deng, Y. Y. Zhao, P. L. Wang, L. L. Xing, Y. Zhang and X. Y. Xue, *Nanotechnology*, 2014, **25**, 265501.
48 W. L. Zang, Y. X. Nie, D. Zhu, P. Deng, L. L. Xing and X. Y. Xue, *J. Phys. Chem. C*, 2014, **118**, 9209-9216.

